Passive scene imaging of absorbing gases by narrowband dielectric filter modulation

D. M. Benton
david.benton@l-3com.com

L-3 TRL Technology, Unit 19 Miller Court, Severn Drive, Tewkesbury, Gloucestershire, GL20 8DN, United Kingdom

This paper examines a method for locating within a scene a distribution of an absorbing gas using a passive imaging technique. An oscillatory modulation of the angle of a narrowband dielectric filter located in front of a camera imaging a scene, gives rise to an intensity modulation that differs in regions occupied by the absorbing gas. A preliminary low cost system has been constructed from readily available components which demonstrates how the location of gas within a scene can be implemented. Modelling of the system has been carried out, especially highlighting the transmission effects of the dielectric filter upon different regions of the image.
[DOI: http://dx.doi.org/10.2971/jeos.2013.13008]

Keywords: Absorption, spectral imaging, modulation

1 INTRODUCTION

Absorption spectroscopy uses specific and unique absorptions within the visible and infra red regions of the spectrum to identify the presence and quantity of specific chemicals. Optical spectroscopy of gases can achieve trace level detection [1] but this is normally through an *active* process where the scene is illuminated by a laser [2]. The use of high intensity tunable sources such as lasers makes this possible but often this leads to other limitations such as a small sampling volume, limited field of view and finite range, to say nothing of concerns such as eye safety, power consumption, covertness and cost. Although target gas concentration levels may be low, the absorption paths can be very long (kms) enabling detection at high sensitivity [3].

Passive techniques [4] rely on changes in the background light levels to expose the presence of the absorbants. Correlation spectrometry is one such passive technique that has been used for measuring trace amounts of atmospheric pollutants such as sulphur dioxide emitted in plumes from volcanoes [5]. More recently this technique has been overtaken by the use of compact miniature spectrometers where the size reduction offers benefits to practical applications of atmospheric monitoring [6, 7].

The use of passive techniques can be difficult due to low light levels (compared to a laser) however there are some significant advantages. With a passive imaging system a wide field of view can be examined constantly without the need for complicated scanning, and thus providing an image of the scene 'as is' rather than being reconstructed. Dispersive elements coupled with 2 dimensional imaging can be used to tie together spectral information with spatial distribution [8]. A coded aperture based spectral imaging system capable of resolving into closely spaced (approx 10 nm) spectral windows has been demonstrated operating across the visible band [9, 10]. Video capture and processing technology has been used for imaging anthropogenic gas distributions [11]–[13] such as NO_2 and SO_2 which has the potential to be useful from satellites.

The motivation behind this work is to produce a low cost technique that is simple to implement and does not require large amounts of reconstruction or data processing. The principle behind the work presented here is to make use of a tunable bandpass filter with a narrow transmission bandwidth, building upon work presented in [14] The filter can be progressively tuned across an absorption feature of the target gas such that the feature falls outside of the transmission profile. Assuming the intensity of background light is essentially constant over the tuning range, an intensity difference in the bandpass transmission will result. By oscillating the filter across the absorption an intensity modulation can be induced when the transmitted light has travelled via the absorbing gas. This technique is normally performed by tuning the source, such as in DIAL or tunable diode laser spectroscopy [2]. By tuning a suitable filter this technique can be applied to an entire image and from this the modulation of regions or individual pixels can be used to detect regions of a scene containing the absorber. However tunable filters with a suitably narrow bandwidth($<$10 nm) are not available. Astronomical spectroscopic applications have used tunable Fabry Perot etalon cameras [15, 16] for imaging with spectroscopic information such as regional velocity. However these devices are fragile and expensive with very narrow bandwidths. Therefore, the approach proposed here utilises a well established optical technique [17] of tilting a dielectric interference filter to translate the pass band to shorter wavelengths. The filter

Received October 22, 2012; revised ms. received November 26, 2012; published January 31, 2013 ISSN 1990-2573

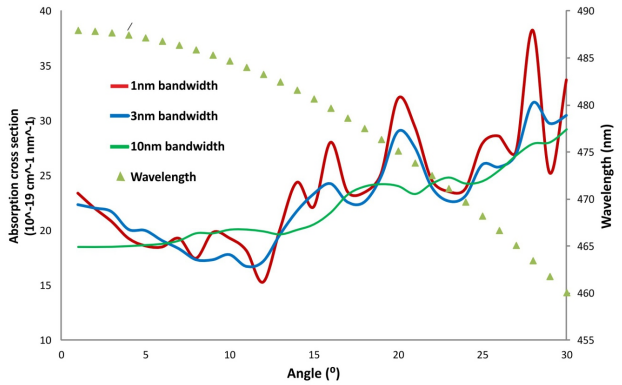

FIG. 1 The integrated absorption cross section for NO_2 as seen through a narrowband filter as a function of tilt angle and filter spectral bandwidth. The central transmission wavelength of the filter is also presented using the right hand scale.

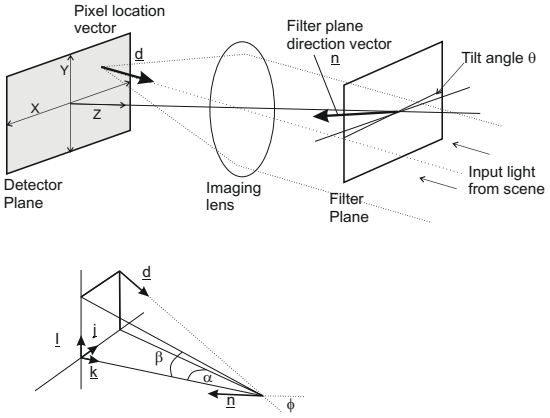

FIG. 2 A diagram representing the relationship between a point in the detector plane and the filter plane.

central transmission wavelength λ as a function of tilt angle ϕ is:

$$\lambda(\phi) = \lambda(0)\sqrt{1 - \left(\frac{1}{n_e}\right)^2 \sin(\phi)^2} \tag{1}$$

where n_e is the effective refractive index [18]. Tilting dielectric filters are a cost efficient and in principle, easily implemented technique and is the basis for the previous work [14].

Nitrogen dioxide is a useful gas with which to test this idea because it has absorption features in the visible region for which narrowband interference filters are readily available. Using data for the absorption cross section of NO_2 [19] around the 490 nm region the integrated absorption cross-sections seen through a filter with bandwidths of 1 nm, 3 nm and 10 nm have been calculated and are shown in Figure 1. The data for a 1 nm width is equivalent to the intrinsic absorption data for NO_2, whereas the 3 nm and 10 nm spectral bandwidths represent commercially available filter options. The angle tilt function as given in Eq. (1) is also shown. From this data it can be seen that the bandwidth should be of the order of the spacing between spectral features in order that variations in cross section are not averaged out by the bandwidth being too wide – as can be seen the 10 nm bandwidth shows less variation in average attenuation (per nm of bandwidth) than the 3 nm bandwidth filters.

2 THE SYSTEM

The simplest arrangement for such a system is to locate the tilting filter directly in front of the camera viewing the scene. This arrangement works and was demonstrated in [14] although the tilting filter induces an image shift that must be corrected (either in software or with a counter-tilting transmissive plate). However this arrangement leads to complications in the interpretation of the image modulation which varies across the scene as follows.

Each point in the image experiences a central filter wavelength dependent upon the angle made to the optic axis and the effective angle of the filter. The relationship between the detector and filter planes is defined in Figure 2. The filter is tilted about the vertical Y axis by an angle θ. The direction chosen should be considered as the line passing from the image point in the detector plane through the centre of the lens to the filter. The angle (ϕ) between the unit vector of the plane ($\boldsymbol{n}$) and the direction vector ($\boldsymbol{d}$) from a pixel is calculated from the dot product of the $\boldsymbol{d}.\boldsymbol{n}$ where

$$\underline{\mathbf{n}} = \underline{\mathbf{i}}\sin(\theta) + \underline{\mathbf{j}}.0 + \underline{\mathbf{k}}\cos(\theta) \tag{2}$$

And

$$\underline{\mathbf{d}} = \underline{\mathbf{i}}\sin(\alpha) + \underline{\mathbf{j}}\sin(\beta) + \underline{\mathbf{k}}\cos(\alpha).cos(\beta) \tag{3}$$

Resulting in

$$\cos(\phi) = \sin(\alpha)\sin(\theta) + \cos(\alpha)\cos(\beta)\cos(\theta) \tag{4}$$

For a camera with a known field of view, the angles α and β are to a good approximation linearly proportional to the pixel location relative to the centre of the sensor, assuming this to be the optical axis of the system. Substituting this angle into Eq. (1) the central transmission wavelength as seen by each pixel can be computed. Modelling for a field of view of 10°with an arbitrary number of pixels we can see the central wavelength transmitted by the filter varies across the image (see Figure 3). Thus a modulation between say 0°and 10°will see a larger wavelength shift on one side of the image, meaning that different parts of the image will be subject to different spectral modulations. Nevertheless this simple technique of oscillating a filter placed in front of a camera was attempted in order to locate an absorbing sample placed in the scene with a view that variations in temporal intensity could be observed, particularly if the absorbing gas has a large number of close proximity spectral features, as most molecular gases do. Results of this approach presented in [14] show the presence of a cylindrical glass absorption cell in a scene, identified using several methods of analysing the time series for each pixel which will be discussed later.

It is of course desirable that each pixel in the image sees the same spectral modulation as this will lead to more consistent results and less processing of the final image to account for position dependent effects. Viewing through a tilted filter is always going to make this a difficult result to achieve The

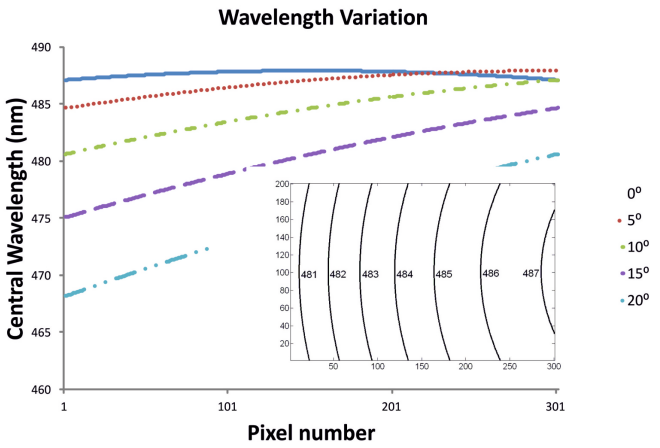

FIG. 3 Central wavelength variation across a field of view of 10 degrees with various filter tilt angles for a filter designed for transmission at 488 nm with no tilt. The number of pixels is chosen arbitrarily for ease of calculation. Inset is a two dimensional representation of the central transmission wavelength contours for a filter tilted at 10°.

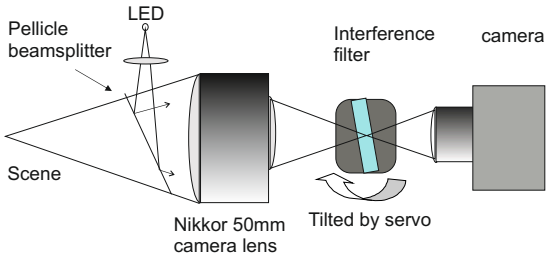

FIG. 4 A schematic diagram of of the experimental setup that focuses through a tilting interference filter.

ideal situation would be to use a narrowband, tunable filter capable of transmitting and affecting an entire image without tilting, but no such cost efficient, readily available technology is known to the author.

One way of reducing the effect of the offset centre wavelength varying across the image is to include an additional imaging lens before the filter, with the filter at the focal plane. The lens requires a focal length short enough such that angular magnification is less than unity. This has the effect of compressing the field of view such that the angle of rays passing through the filter is reduced and the resulting offset of central transmission wavelength is significantly reduced due to the non-linear relationship shown in Eq. (1).

The experimental arrangement is shown in Figure 4. Focussing into the filter is achieved using a 50 mm Nikkor camera lens, which allowed the F-number to be controlled which also controls the spectral width contained within the image. This lens had the advantage of a large collection area (50 mm diameter) which was used to concentrate the light through the smaller 25 mm diameter dielectric filter, thereby producing a brighter image in the camera. A pellicle beamsplitter is used to introduce light from an LED into the scene. This is subsequently used to correct for the image shifts caused by tilt of the filter by checking a portion of the scene for the bright circle from the LED and shifting individual frames to a common position. The filter is supported upon a servo (Robotis RX 10)

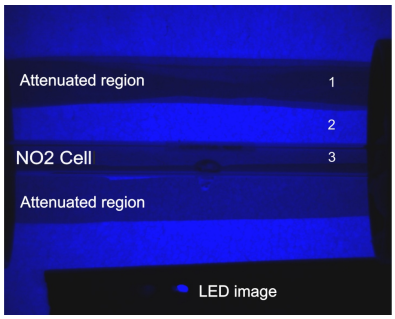

FIG. 5 The scene as viewed through a 490 nm filter with a 10 nm bandwidth. Region 1 is a neutrally attenuated region, region 2 is not attenuated and region 3 contains the absorbing gas cell.

which is being oscillated under computer control via a LabView program. After passing through the interference filter the light is captured by a USB camera (ThorLabs DCU224C) with a 25 mm diameter lens (focal length 25 mm) and the frames stored in a buffer. When a predetermined number of frames are present in the buffer frame capture is paused while the frame buffer is corrected for image shift and then the time series for each pixel is processed. The scene itself contained a glass cell containing NO_2, chosen because it has spectral features in the visible part of the spectrum where narrowband dielectric filters are readily available

Observation of the desired modulation in the time series intensity is complicated by a global intensity modulation across the image as the filter is tilted. To extract a modulation arising from absorbing gas present in the image it was felt desirable to define a reference signal that represented the modulation where no absorption was present and then compare the time series for each pixel with this reference signal. In principle the light from the LED would be well suited for this purpose as it has not originated from within the scene, however the 3 component structure of a white light LED as used here shows strong intensity variation between 460 nm and 490 nm, the spectral region viewed here and hence is not appropriate for use as a reference. Instead a region of the image known not to contain the absorbing gas was selected and the average intensity calculated and used as the reference signal.

3 RESULTS

The scene being viewed consisted of a horizontal cylindrical absorption cell containing NO_2 at 400 mBar in a 6 mm diameter tube. The scene was back illuminated through a diffuser and the cell appeared as a dark stripe in the scene. Additional horizontal strips of neutral attenuating material were also incorporated so as offer a level of comparison between spectrally absorbing and neutrally absorbing 'dark' features in the scene. The scene as viewed through the filter is shown in Figure 5, where the attenuating regions, the LED image and cell support region(black) can also be seen.

For each pixel location a time series was created from the intensity value in each frame. The time series for each pixel was constructed after frame realignment had taken place, to compensate for the image shift. Each time series was then nor-

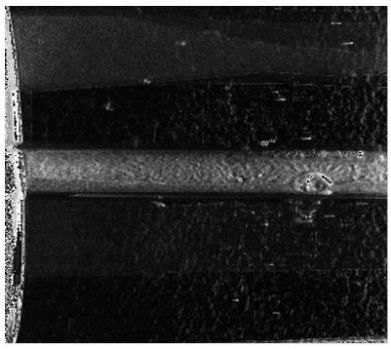

FIG. 6 The processed scene (cropped to remove the LED region) clearly showing the absorption cell.

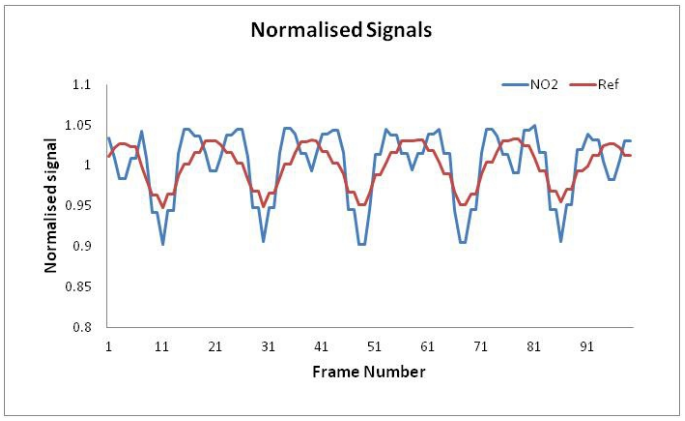

FIG. 7 Normalised time varying intensities extracted from a reference region and an NO_2 absorbing region.

malised by its mean level in order to account for differences in intensity across the scene. Each normalised time series was processed to give a single value representing the amount of modulation in comparison to the reference. A resultant image was then formed from the processed values for each pixel. Earlier work established that the following statistical comparisons between the time series signal (S) and the reference signal (R) were able to expose absorption based modulations:

The Covariance coefficient:

$$cov\,(\mathrm{S},\mathrm{R}) = \sum_{i=1}^{n} \frac{[(S_i - \bar{S})]\,(R_i - \bar{R})}{n}. \tag{5}$$

The Pearson Correlation coefficient:

$$r\,(S,R) = \frac{cov(S,R)}{\sigma_S \sigma_R}, \tag{6}$$

where σ is the sample variance. And a covariance operating on related variables:

$$cov\left(S - R, \frac{1}{R}\right). \tag{7}$$

This covariant relationship was found appropriate to the structure of the absorption based modulation. Whilst these operations can reveal the absorbing-modulating regions in an image, the values of the resulting scalar coefficients is in general small and contrast enhancements of the final processed image are required to reveal the small difference between the processed pixel time series. This arises from the tendency for the both the reference data and the absorption data to cancel itself when summed over an oscillation period. A more appropriate time series operation is to evaluate the sum of the differences of the squares

$$f(S,R) = \sum_{i=1}^{n} (S_1^2 - R_i^2), \tag{8}$$

which will only increase over the course of an oscillation period and will increase with integration times longer than a single period.

Time series processing using Eq. (8) was performed upon the scene of Figure 5 using a filter with a 3 nm bandwidth centred around 488 nm. The filter was oscillated with a linear ramp between 10°and 20°in order to modulate from the lowest absorption value to a significantly higher value, thus enhancing the scale of modulation depth (see Figure 1). A 3 nm bandwidth spectral filter significantly attenuates the input light levels and long frame integration times limited the frame rate to 6 frames per second. The filter was typically oscillated at a rate of 0.5 Hz to ensure sufficient samples (frames) per cycle. Servo control, video capture and time series processing was all controlled using a LabView program. The result of the processing is shown in Figure 6 where a cropped version shows the absorption cell clearly as a central horizontal stripe. This feature stands out with no significant features in the similar looking attenuated regions. This was intended to show that dark features alone are not being highlighted by the processing. However, the average intensity of a time series can have an influence. The narrow bandwidth of the filter results in the intensity reaching the camera sensor being quite low and in this case located approximately 95% in the blue channel. Thus dark objects, such as the support regions for the absorption cell at the sides of the scene, are dominated by noise (a situation made worse by the high gain setting needed). Because the time series is normalised to the mean intensity, the quantisation of noise in very low intensity regions appears as large changes and can make a significant contribution to the processed value of the time series, often significantly stronger than the absorption effect. To overcome this effect a time series was zeroed if its mean level was low and its variance was greater than 20% of the mean.

Time series data captured from an absorbing region and the reference signal are shown in Figure 7 for an exaggerated tilt between 0°and 30°and it is clear from this that absorbing regions should show a different signature than regions without an absorber present. Examination of Figure 1 shows that between 10°and 20°we would expect the transmitted intensity from an absorbing region to show maximum fluctuation as the absorption cross section increases significantly and then decreases. In comparison with the reference signal the time series for an absorbing region would show more structure and this leads to larger values when processed via Eq. (8).

Taking a horizontal line of pixels, which in this case represents the same scene constitution (i.e. absorber, neutral) the statistical variance of the time series for each pixel was calculated. The distribution of variance values at each pixel location for pixels in a horizontal line within different regions is shown in

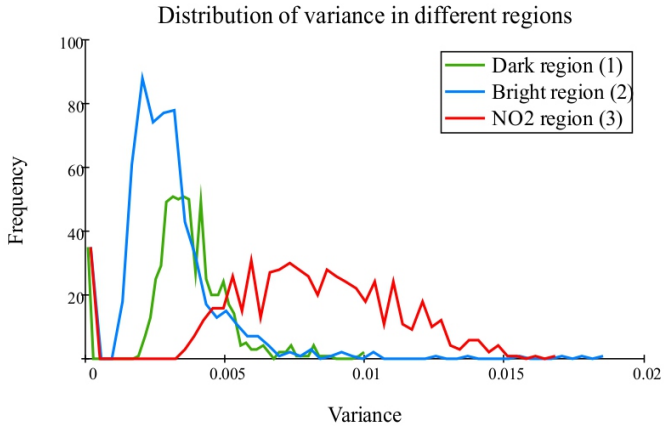

FIG. 8 Time series variance for 3 regions within the scene.

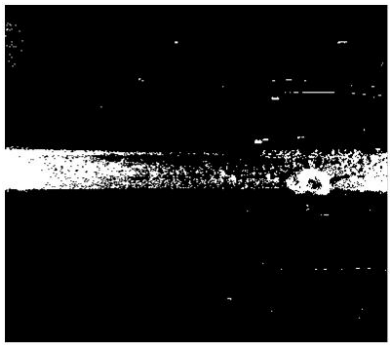

FIG. 9 Processing of the scene containing an NO_2 cell simply examining the variance of the time series data.

Figure 8, where the vertical scale of frequency represents the number of occurrences of the variance values (horizontal axis) within the line of pixels chosen. Each line of pixels is within regions 1, 2 and 3 as labelled in Figure 5, corresponding to a bright region(1) , a dark attenuated region(1) and the NO_2 absorbing region(2). It is clear from this figure that the statistical variance in the NO_2 region is larger than in other regions. It is therefore clear that this statistical variance is the underlying property that is being discriminated when the time series are processed using Eqs. (5)–(8). To confirm this the experiment was repeated but processing involved just the determination of the variance of the time series for each pixel location with the resulting processed image shown in Figure 9.

The focussing effect of the collecting lens through the filter will effectively broaden the spectral bandwidth. The contribution to the bandwidth can be determined from the half angle calculated from the F-number of the lens and then using the central wavelength shift from Eq. (1). This reveals that an F-number of 2.8 has a half angle of 9.8°which produces an increase in spectral bandwidth comparable to the inherent bandwidth of the filter. A basic model was constructed to understand the signal variation expected from the effect of an increased spectral absorption profile.

The signal level S, at a point in the image plane of the camera, originating from a point in the object space will be dependent upon the following factors: The source radiance function $R(\lambda)$ which is dependent upon wavelength; The geometrical collection efficiency of the system G including losses; The filter spectral transmission function $F(\lambda)$ and the detector efficiency $D(\lambda)$. There is also noise N, arising from shot noise generated in the semiconductor detector which is a function of the square root of the signal intensity and readout noise from the circuitry.

$$S = R(\lambda) * G * F(\lambda) * D(\lambda) + N(\sqrt{S})$$

By considering regions in the object space with similar levels of intensity, such as the NO_2 region and a neutrally dark region the statistical nature of noise in both regions will be the same and all other contributions are the same except for the source function. In this case the spectral variation of the absorption function modifies the source function to give rise to temporal variation. Therefore the difference in variance arises from the absorption modulation function. In brighter regions the relative signal to noise is higher and the variance is lower for the normalised signals, as can be seen in Figure 8.

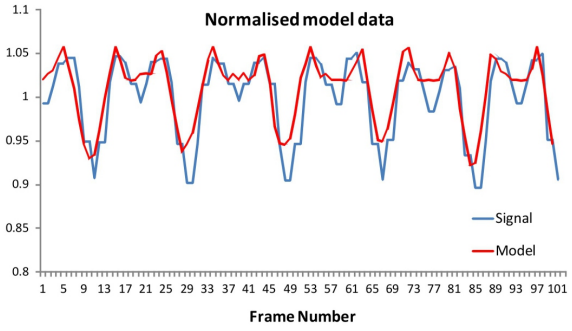

FIG. 10 Captured and Modelled data for the absorption signal for a filter tilt of 0°-30.

According to the specifications the spectral response of the camera shows a near linear decrease of 40% between 500 nm and 400 nm. As the angle of tilt of the filter is changed linearly this results in a non linear variation of central transmission wavelength and hence in camera response in accordance with Eq. (1) and this generates the variation seen in the reference signal. Using tilt angle values for the data in Figure 7 the reference signal was modelled using Eq. (1) and is a representation of the detection responsivity. The variation in absorption signal was generated using the attenuation values calculated for Figure 1 and using the detection efficiency values obtained from fitting to the reference. Figure 10 shows the absorption signal for a filter tilt between 0°and 30° along with the modelled signal expected from the attenuation values. Fitting of this data was used to determine the effective spectral width of the system to be 5 nm, with thus a 2 nm width contribution arising from the focussing effect of the collection lens operating at F#4, as would be expected from calculation of the half angle of the marginal rays.

3.1 CONCLUSIONS

The motivation behind this work was to demonstrate that it is possible to identify regions of a scene as containing a specific absorbing material using a relatively low cost method with a fairly simple implementation – intentionally in contrast to expensive data intensive methods such as hyperspectral imaging. The work shown here is introductory and intended to prove the principle of the idea and identify the key characteristics of the technique. The simplest implementation - that of an oscillating filter in front of a camera - is shown to be limited by the nonlinear change in transmission wavelength caused at the extreme angle of filter tilt and the edge of the field of view. Reducing the angular magnification is effective but clearly the best approach, where possible, should be to use a telecentric imaging system before the filter. The choice of filter central wavelength employed to give the largest discrimination through changes in absorption cross section would also be advantageous, in this work the offset of central wavelength from absorption feature resulted in significant tilt angles. A better approach would be to use a narrowband electronically tunable filter, such as a pair of liquid crystal tunable filters with central wavelengths offset to result in a transmission bandwidth that is narrower than a single filter, which would remove the need for mechanical tilting. It is hoped that this approach can be implemented in the future. However it should be noted that this adds a significant increase in cost to the system and is only applicable to the visible part of the spectrum, whereas dielectric filters are available well into the infra red, where many more spectral signatures are to be found. Further development work is needed to implement the improvement deemed desirable from this work in order to see the technique implemented upon a real world scene where it could find use as an environmental / pollution monitoring tool. Further development of the processing technique is required to make use of the intrinsic statistical nature of the signal and to help determine the detection limits of this technique.

References

[1] U. Platt, "Modern methods of the measurement of atmospheric trace gases," Phys. Chem. Chem. Phys. **1**, 5409–5415 (1999).

[2] W. Demtröder, *Laser spectroscopy: basic concepts and instrumentation* (Springer, Berlin, 2003).

[3] R. T. Ku, E. D. Hinkley, and J. O. Sample, "Long-Path Monitoring of Atmospheric Carbon Monoxide with a Tunable Diode Laser System," Appl. Optics **14(4)**, 854–861 (1975).

[4] M. W. Sigrist, *Air monitoring by spectroscopic techniques* (Wiley, New Jersey, 1994).

[5] P. M. Hamilton, R. H. Varey, and M. M. Millan, "Remote sensing of sulphur dioxide," Atmos. Eviron. **12**, 127–133 (1978).

[6] T. Elias, A. J. Sutton, C. Oppenheimer, K. A. Horton, H. Garbeil, V. Tsanev, A. J. S. McGonigle, and G. Williams-Jones, "Comparison of COSPEC and two miniature ultraviolet spectrometer systems for SO2 measurements using scattered sunlight," B. Volcanol. **68**, 313–322 (2006).

[7] B. Galle, C. Oppenheimer, A. Geyer, A. J. S McGonigle, M. Edmonds, and L. Horrocks, "A miniaturized ultraviolet spectrometerfor remote sensing of SO2 fluxes: a new tool for volcano surveillance," J. Volcanol. Geoth. Res. **119**, 241–254 (2002).

[8] J. M. Mooney, V. E. Vickers, M. An, and A. K. Brodzik, "High throughput hyperspectral infrared camera," J. Opt. Soc. Am. A **14**, 2951–2961 (1997).

[9] A. Wagadarikar, N. Pitsianis, X. Sun, and D. Brady, "Video rate spectral imaging using a coded aperture snapshot spectral imager," Opt. Express **17(8)**, 6368–6388 (2009).

[10] A. Wagadarikar, N. Pitsianis, X. Sun, and D. Brady, "Spectral image estimation for coded aperture snapshot spectral imagers," Proc. SPIE **7076**, 795545 (2008).

[11] M. Pujadas, J. Plaza, J. Teres, B. Artinao, and M. Millan, "Passive remote sensing of nitrogen dioxide as a tool for tracking air pollution in Urban areas: the Madrid urban plume, a case of study," Atmos. Environ. **34(19)**, 3041–3056 (2000).

[12] V. S. Davydov, and A. V. Afonin, "Developing video spectroradiometer–gas-viewers for determining the spatial distribution of anthropogenic gases in the near-earth atmosphere and the results of a full-scale experiment," J. Opt. Technol. **74(2)**, 100–106 (2007).

[13] A. V. Afonin, N. M. Drichko, and I. N. Sivyakov, "Wide-angle interference-polarization filter of a video spectroradiometer-gas viewer for recording nitrogen dioxide," J. Opt. Technol. **71**, 776–779 (2004).

[14] D. Benton, "Technique for passive scene imaging of gas and vapor plumes using transmission-waveband modulation," Opt. Eng. **51(5)**, 050501 (2012).

[15] T. J. Kentischer, W. Schmidt, M. Sigwarth, and M. v. Uexkull, "TESOS, a double Fabry-Perot instrument for solar spectroscopy," Astron. Astrophys. **340**, 569–578 (1998).

[16] G. Joncas, and J.-R. Roy, "A fabry Perot camera for the study of galactic nebulae: instrumentation and reduction of digitized interferograms" Publ. Astron. Soc. Pac. **96**, 263–270 (1984).

[17] S. A. Pollack, "Angular Dependence of Transmission Characteristics of Interference Filters and Application to a Tenable Fluorometer," Appl. Optics **5**, 1749 (1966).

[18] J. R.Barry, and J. M. Kahn, "Link design for non-directed Wireless Infrared Communications," Appl. Optics **34(19)**, 3764–3776 (1995).

[19] A. C. Vandaele, C. Hermans, P. C. Simon, M. Roozendael, J. M. Guilmot, M. Carleer, and R. Colin, "Fourier transform measurement of NO2 absorption cross-section in the visible range at room temperature," J. Atmos. Chem. **25**, 289–305 (1996).